DTU Library

H∞ Robust Current Control for DFIG Based Wind Turbine subject to Grid Voltage Distortions

Wang, Yun; Wu, Qiuwei; Gong, Wenming; Gryning, Mikkel Peter Sidoroff

Published in:
IEEE Transactions on Sustainable Energy

Link to article, DOI:
10.1109/TSTE.2016.2621418

Publication date:
2016

Document Version
Peer reviewed version

Citation (APA):
Wang, Y., Wu, Q., Gong, W., & Gryning, M. P. S. (2016). H∞ Robust Current Control for DFIG Based Wind Turbine subject to Grid Voltage Distortions. *IEEE Transactions on Sustainable Energy*, *8*(2), 816 - 825. https://doi.org/10.1109/TSTE.2016.2621418

H_∞ Robust Current Control for DFIG Based Wind Turbine subject to Grid Voltage Distortions

Yun Wang, Qiuwei Wu, *Senior Member, IEEE*, Wenming Gong, and Mikkel Peter Sidoroff Gryning

Abstract**--This paper proposes an H_∞ robust current controller for doubly fed induction generator (DFIG) based wind turbines (WTs) subject to grid voltage distortions. The controller is to mitigate the impact of the grid voltage distortions on rotor currents with DFIG parameter perturbation. The grid voltage distortions considered include asymmetric voltage dips and grid background harmonics. An uncertain DFIG model is developed with uncertain factors originating from distorted stator voltage, and changed generator parameters due to the flux saturation effect, the skin effect, etc. Weighting functions are designed to efficiently track the unbalanced current components and the 5*th* and 7*th* background harmonics. The robust stability (RS) and robust performance (RP) of the proposed controller are verified by the structured singular value μ. The performance of the H_∞ robust current controller was demonstrated with a 1.5 MW DFIG model, showing its harmonics suppression ability with DFIG parameter perturbation and improved robustness.**

Index Terms**—Doubly fed induction generator (DFIG), grid harmonics, grid voltage distortion, robust control, wind turbine.**

NOMENCLATURE

A. Subscripts

abc	Stationary A, B, and C phases
d, *q*	Synchronous *d*- and *q*-axis
n	The *n*th order of harmonics (*n*= 3, 4, 5, 6, 7)
s, *r*	Stator and rotor
α, β	Stationary α- and β-axis

B. Superscripts

*	Reference value for controller
.	Differential operation

This work was supported in part by National Natural Science Foundation of China (grant number 51407118) and in part by Shenzhen Government Science Foundation (JCYJ20140509172609161, GJHZ20130408173747552).

Y. Wang is with the College of Mechatronics and Control Engineering, Shenzhen University, Nanhai Ave 3688, Shenzhen 518060, China (e-mail: wangyun@szu.edu.cn).

Q. Wu is with the Centre for Electric Power and Energy (CEE), Department of Electrical Engineering, Technical University of Denmark (DTU), 2800 Kgs. Lyngby, Denmark and also with the School of Electrical Engineering, Shandong University, Jinan 25000, China (e-mail: qw@elektro.dtu.dk).

M. Gong is with Electric Power Research Insinuate, China Southern Power Grid, Guangzhou 510080, China (e-mail: gongwm@csg.cn).

M. P. S. Gryning is with DONG Energy, Gentofte 2820, Denmark (e-mail: migry@dongenergy.dk).

C. Parameters and variables

1) DFIG

F	Vector represents current or voltage of DFIG
L_{lr}, L_{ls}	Rotor and stator leakage inductances
L_m, L_r, L_s	Mutual, rotor and stator inductances
P , Q	Wind turbine output active and reactive powers
R_r, R_s	Rotor and stator resistances
U_r	Modulating voltage for rotor side converter
i_r, i_s	Rotor and stator currents
u_{dc}	DC-link voltage
u_r, u_s	Rotor and stator voltages
ω	Angular frequency
ω_B, ω_{slip}	Nominal, slip electrical angular frequencies
ω_r, ω_s	Rotor and stator electrical angular frequencies
θ_r, θ_s	Phase angels of rotor and stator voltage vectors

2) State-space

A, B_1, B_2	Parameter matrixes of plant state-space
B_d	Parameter matrixes of external disturbance
C, D	Parameter matrixes of plant state-space
G, K, P	Plant, controller, generalized plant models
$\boldsymbol{d}$, $\boldsymbol{r}$, $\boldsymbol{u}$	Disturbances, reference inputs, control signals
$\boldsymbol{v}$, $\boldsymbol{x}$, $\boldsymbol{y}$	Controller inputs, plant states, plant outputs
y_Δ, u_Δ	Input and output vectors of Δ
$\boldsymbol{w}$, $\boldsymbol{z}$	Exogenous inputs and outputs
Δ	Diagonal matrix with all system uncertainties

3) H_∞ controller

I	Nominal matrix
K	State space realization of the H_∞ controller
N	System with P, K and their interconnections
$N_{11,12,21,22}$	Blocks of the state-space realization of N
M	Equal to N_{11}
P	Shaped generalized plant model
$P_{11,12,21,22}$	Blocks of the state-space realization of P
S	System sensitivity function
W_u	Weighting function of H_∞ controller outputs
W_p	Weighting function of H_∞ controller inputs
det()	Determinant of a Matrix
diag{}	Diagonal matrix
$\bar{\delta}$	Peak of the singular value of a matrix

4) PIR controller

K_I	Integral parameter
K_P	Proportional parameter
K_{Ri}	Resonant parameter of the *i* th harmonic
s	Laplace coefficient
ω_{ci}	The *i*th cut-off frequency of the resonant factor

ω_i The ith harmonic frequency

I. INTRODUCTION

WIND turbines (WTs) are increasingly integrated into weak grids such as the collector system of offshore wind farms and distribution networks. Due to the existence of reactive power compensation equipment, nonlinear load, unbalanced load, etc., grid voltage distortions occur more frequently, including grid background harmonics (typically the 5*th* and 7*th* harmonics) [1]-[2] and unbalanced grid voltages due to asymmetric faults or other causes [3]. Grid codes in many countries require that WTs stay connected and maintain output currents quality under a certain range of grid voltage distortions [4]-[5]. In this regard, higher harmonics suppression ability and stability are required.

Doubly fed induction generator (DFIG) based WTs have many advantages such as lower cost, smaller size, and smaller power electronics capacity [6]. However, the DFIG is more sensitive to grid voltage distortions and the impact is more harmful. The impact of grid voltage distortions on the DFIG have been intensively studied [7]-[8]. Because the stator windings are directly connected to the grid, the stator voltage of DFIGs can be directly distorted. Distorted stator voltage will cause both stator and rotor currents harmonics, and induce a significant electromagnetic torque oscillation [7]-[9]. The grid voltage distortions can cause a series of problems on the DFIG, such as overheat of the generator windings and the drive-train damage. Moreover, the generator parameters tend to change under grid voltage distortions, due to the windings overheat with unbalanced currents, the change of flux density and the flux saturation effect [10]-[11]. Therefore, the parameter perturbation of the DFIG brings another challenge to the generator control system under grid voltage distortions, and its control performance and stability will become worse.

As [7]-[15] show, the mitigation of the effects of grid voltage distortions mainly depends on the DFIG current control. Various current control strategies have been developed to deal with grid voltage distortions. The commonly used scheme is adding more regulators to the conventional proportional integral (PI) regulator. The typical methods are dual-currents control, PI plus resonant (PIR) control and P plus resonant (PR) control [7], [8]-[13]. The resonant regulator can track the AC reference signal at the resonant frequency, such that the PR/PIR controller does not require the decomposition of positive and negative sequence components. The PR/PIR controller shows better performance than the dual-currents control and is widely used to suppress harmonics under grid voltage distortions [7], [12]-[15].

During a grid voltage distortion, there are several orders of currents harmonics to be suppressed simultaneously. Therefore, parallel resonant regulators with corresponding harmonic frequencies are required. The parameters tuning of parallel resonant controllers is iterative because the frequency characteristics at different resonant frequencies interact with each other. As [13]-[14] investigated, without adding phase correction, the system is easy to be unstable. Several resonant parameter tuning methods have been proposed [14]-[15]. The PIR controller design and tuning are based on the classical single-input single-output (SISO) control theory, and depend on the certain model of the generator, which is usually simplified as a first order nominal model in the DFIG current control design [7], [8], [15], [16]. The system robust stability (RS) and robust performance (RP) with the DFIG parameters perturbation are not considered. Therefore, a well-tuned PIR controller can achieve good performance for the nominal model and may achieve acceptable performance for a non-nominal system if it has enough stability margins. However, the robust performance for all the possibilities of the uncertain system cannot be guaranteed. A few other methods such as sliding mode control [17]-[18], repetition control [19]-[20] and predictive direct power control [21]-[22] have been used under grid voltage distortions. However, the parameters perturbation and robustness are not fully considered.

The H_∞ robust control has been successfully used in many electrical control fields such as voltage source inverter (VSI) [23], dynamic voltage restorer (DVR) [24], uninterruptible power supplies [25], etc. As an advanced control method, the controlled system of the H_∞ robust control is uncertain and can be a multi-input multi-output (MIMO) structure. The system RS and RP performance can be guaranteed by introducing the H_∞ norm to constrain all the possibilities of the uncertain system into a bound [26]-[27]. In this paper, an H_∞ robust rotor current controller is developed for the DFIG based WTs to realize rotor current harmonic suppression and improve its RS and RP subject to grid voltage distortions and parameter perturbation.

The main contributions of this paper are: (A) develop an uncertain DFIG model for robust rotor current control; (B) propose rotor current control requirements for DFIG based WTs subject to grid voltage distortions and generator parameter perturbation; (C) develop an H_∞ rotor current controller to suppress multiple harmonics of the 2*nd*, 4*th* and 6*th* orders simultaneously and guarantee the system RS and RP under grid voltage distortions and DFIG parameter perturbation.

The paper is organized as follows. Section II describes an uncertain MIMO DFIG model, analyzes the influence of the grid voltage distortions on the rotor currents, and proposes the control requirements. In Section III, the H_∞ rotor current controller is designed, including the weighting function design and parameter tuning, and the RS and RP are validated by the structured singular value μ. Case studies are presented in Section IV to demonstrate the harmonic suppression performance and the robustness of the developed H_∞ controller under grid voltage distortions with parameter perturbation, followed by conclusions.

II. UNCERTAIN MODEL AND CONTROL REQUIREMENTS

A. Uncertain system model

The whole system modeling consists of the DFIG based WT model and the network model. The mitigation of the impact of grid voltage distortions mainly depends on the rotor current loop control [7]-[8], so the WT model focuses on the generator. Compared with the rapid current response of the generator, the responses of the speed control loop and the mechanical part are slow. Therefore, the wind speed of the DFIG WT is regarded as constant. The grid structure and parameters influence the harmonics order, the total harmonic distortion (THD) [2] and the voltage dip depth [28], which do not affect the controlled system. Therefore, the network model at the generator side is usually considered as a controlled voltage source, with harmonics and unbalanced distortions [7]-[8], [15]-[23], [16], [33]-[29]. Based on the basic DFIG model in the time domain [6], a 4*th* order generator model at the synchronously rotating dq frame can be described by the state-space realization in (1), marked as *G*. All the model parameters used in this paper are listed in the Appendix.

$$\begin{cases} \dot{\boldsymbol{x}} = A\boldsymbol{x} + [B_1, B_2][\boldsymbol{u}, \boldsymbol{d}]^T \\ \boldsymbol{y} = C\boldsymbol{x} + D\boldsymbol{u} \end{cases} \tag{1}$$

where $\boldsymbol{x} = [i_{sd}\ i_{sq}\ i_{rd}\ i_{rq}]$, $\boldsymbol{y} = [i_{rd}\ i_{rq}]$, $\boldsymbol{u} = [u_{rd}\ u_{rq}]$ and $\boldsymbol{d} = [u_{sd}\ u_{sq}]$. All variables and parameters are transformed into the nominal system and the parameter matrixes are,

$$A=\frac{\omega_B}{L_m^2-L_rL_s}\begin{bmatrix} L_rR_s & L_m^2\omega_{slip}-L_sL_r\omega_s & -L_mR_r & -L_mL_r\omega_r \\ L_sL_r\omega_s-L_m^2\omega_{slip} & L_rR_s & L_mL_r\omega_r & -L_mR_r \\ -L_mR_s & L_sL_m\omega_r & L_sR_r & L_m^2\omega_s-L_sL_r\omega_{slip} \\ -L_sL_m\omega_r & -L_mR_s & L_sL_r\omega_{slip}-L_m^2\omega_s & L_sR_r \end{bmatrix}$$

$$B_1=\frac{\omega_B}{L_m^2-L_rL_s}\begin{bmatrix} L_m & 0 \\ 0 & L_m \\ -L_s & 0 \\ 0 & -L_s \end{bmatrix},\ B_2=\frac{\omega_B}{L_m^2-L_rL_s}\begin{bmatrix} -L_r & 0 \\ 0 & -L_r \\ L_m & 0 \\ 0 & L_m \end{bmatrix},\ C=\begin{bmatrix} 0 & 0 & 1 & 0 \\ 0 & 0 & 0 & 1 \end{bmatrix},\ D=0$$

The system uncertainties focus on two aspects in this paper. One is the DFIG parameter perturbation. The other is the grid voltage disturbance. The DFIG parameter perturbation refers to the uncertainties of L_m, L_{ls}, L_{lr}, R_r. Each parameter uncertain range is $(\pm 50\%)$ which can include all the possible parameters perturbation [10]-[11]. The uncertain parameters and matrixes of (1) are reorganized as the nominal part plus its uncertain part, i.e. $L_m+\Delta L_m$, $A+\Delta A$.

The grid voltage disturbance can be described by an H_∞ norm. The H_∞ norm means the maximum amplitude or energy from any input variable to the output variable of an MIMO system [30]. By describing the distorted grid voltage as $(1+\delta\boldsymbol{d})\boldsymbol{d}$ with a multiplicative factor marked as $\delta\boldsymbol{d}$, if $\delta\boldsymbol{d} = (\pm 100\%)$, it satisfies $\|(1+\delta\boldsymbol{d})\boldsymbol{d}(w)\|_\infty \le 2$. It means the largest gain of uncertain grid voltage is 2 pu. Based on the grid background harmonics analysis [1]-[2] and the grid voltage unbalance analysis [28], the range of the distorted grid voltage variation is between 1 ± 1 pu, so it can describe all the possibilities of grid voltage distortions. Equation (1) can be further described as (2) with uncertainties. The structure diagram of the uncertain system is shown in Fig. 1.

$$\begin{cases} \dot{\boldsymbol{x}} = (A+\Delta A)\boldsymbol{x} + (B_1+\Delta B_1)\boldsymbol{u} + (B_2+\Delta B_2)(1+\delta d)\boldsymbol{d} \\ \boldsymbol{y} = C\boldsymbol{x} + D\boldsymbol{u} \end{cases} \tag{2}$$

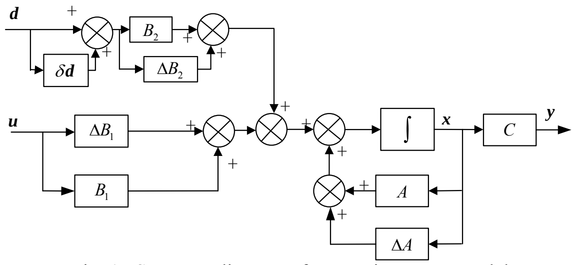

Fig. 1. Structure diagram of uncertain system model

Fig. 2 shows the frequency characteristics of the uncertain controlled system. The uncertainty of the system is defined as a parameter interval. The Bode plots represent sampled values of the system parameters within that interval. The Bode diagrams are from u_{sd}, u_{sq}, u_{rd} and u_{rq} to i_{rd}, respectively. The curves marked with '*' are obtained with the nominal model, and other curves are for the uncertain models with different parameter perturbation. It is seen the frequency characteristics of i_{rd} have a range of variations between the nominal model and uncertain models, indicating the DFIG parameter perturbation and the input grid voltage disturbance have influence on the controlled system.

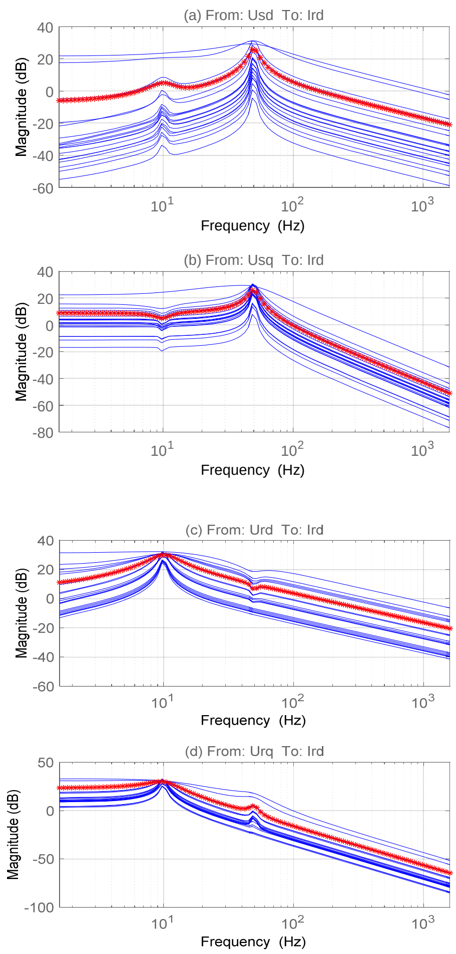

Fig. 2. Bode plots of the uncertain system model

B. Grid voltage distortion and control requirements

WTs usually connect to a three-phase three-wire network through step-up transformers. Therefore, the background harmonics of the stator voltage under grid voltage distortions do not have zero-sequence component. The unbalanced fundamental stator voltage can be decomposed into positive-sequence and negative-sequence parts of the fundamental frequency. The 5th and 7th harmonics of stator voltage are also considered. So in the *dq* rotating coordinates, the DFIG current vector, marked as *F*, can be decomposed into the 2nd, 4th and 6th harmonics as (3) shows [7]-[8].

$$F_{dq}(t) = F_{dq+} F_{dq2}e^{j2\omega t} + F_{dq4}e^{j4\omega t} + F_{dq6}e^{j6\omega t} \tag{3}$$

Fig. 4 shows the Fast Fourier Transform (FFT) analysis of the rotor current subjected to a distorted grid voltage condition shown in Fig. 3. Because the current responses of the *d* and *q* axes are similar, only i_{rd} is shown. The fundamental frequency is 50 Hz. It is seen that, under the grid voltage distortion with a single phase voltage drop to 50% together with 10% of the 5*th* and 10% of the 7*th* background harmonics, the 100 Hz, 200 Hz and 300 Hz harmonic currents are excited.

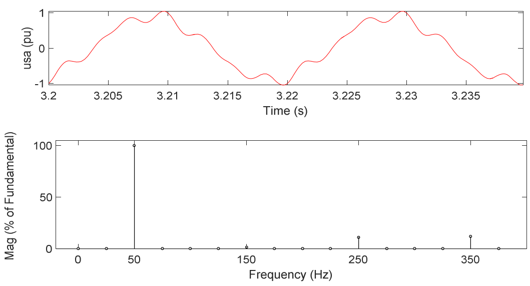

Fig. 3. FFT analysis of a specific grid voltage distortion

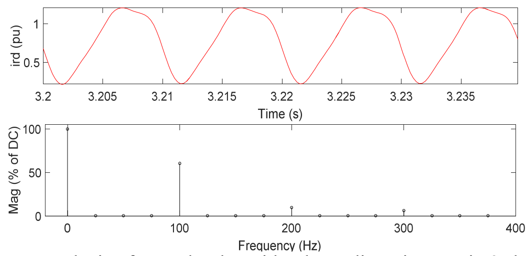

Fig. 4. FFT analysis of i_{rd} under the grid voltage distortion as Fig.3 shows

Based on the above analysis, and considering the DFIG parameter perturbation and recommendations for harmonics control in electrical power systems [31], the rotor current control requirements under grid voltage distortions are proposed as follows.

1) Guarantee tracking performance to the fundamental. Depends on the switching frequency of the PWM modulation, the bandwidth of the current controller commonly is set as 0.1 to 0.2 of the switching frequency. The acceptable bandwidth of the designed controller is *0.4 kHz to 1 kHz*.

2) Suppress harmonics of rotor currents under grid voltage distortions. Rotor currents satisfy *THD* $\leqslant$ *5%*, with the grid background harmonics and unbalanced grid fault occurring simultaneously.

3) Guarantee system robustness under DFIG parameter perturbation, including RS and RP. The DFIG parameter perturbation refers to L_m, L_{ls}, L_{lr} and R_r, with each uncertainty range is ($\pm$50%). The rotor currents satisfy *THD* $\leqslant$ *5%* subject to grid voltage distortions with parameter perturbation.

III. H$_\infty$ Controller Design

A. Controller structure design

Fig. 5 shows the control structure of the rotor side converter (RSC) in the *dq* synchronously rotating coordinates. In Fig. 5, the rotor current controller *K* is designed based on the H$_\infty$ control method. The design of the H$_\infty$ controller *K* is based on the *NΔ*-structure which is illustrated in Fig. 6, where $B_d = B_2 / B_1$. The *NΔ*-structure is a typical description of an uncertain system structure for the H$_\infty$ controller synthesizing design [30]. Each perturbation of the original system shown in Fig 1 can be collected, classified and transformed into a block diagonal matrix marked as *Δ*. *Δ* is described as *diag* $\{\Delta_1, \Delta_1, \ldots \Delta_{14}\}$, including ΔL_r, ΔL_m, ΔL_s, ΔR_r, $\Delta L_m \Delta R_r$, $\Delta L_s \Delta R_r$, $\Delta L_m{}^2\omega_s$-$\Delta L_s \Delta L_r \omega_s$, $\Delta L_r \Delta R_s$, $\Delta L_m \Delta L_r \omega_r$, $\Delta L_m \Delta R_s$, $\Delta L_s \Delta L_m \omega_r$, $\Delta L_r \delta d$, $\Delta L_m{}^2\omega_s$-$\Delta L_s \Delta L_r \omega_{slip}$ and $\Delta L_m \delta d$. *Δ* satisfies $\|\Delta\|_\infty \leq 1$. The input vector of *Δ* is marked as $\boldsymbol{y}_\Delta$, and the output vector of *Δ* is marked as $\boldsymbol{u}_\Delta$.

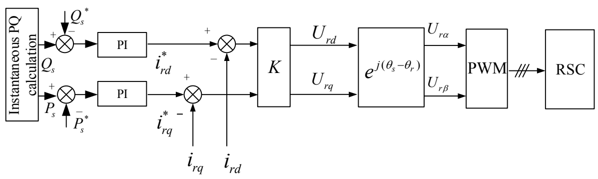

Fig. 5. Control structure diagram of RSC with *K*

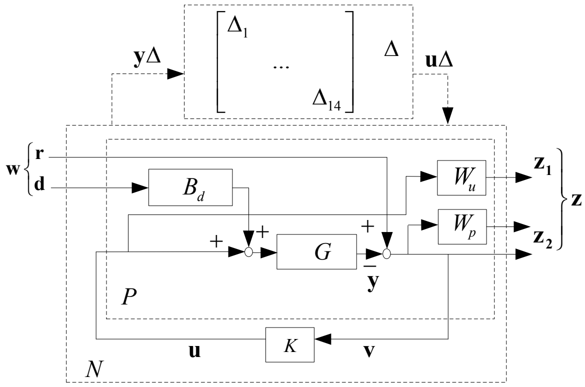

Fig. 6. Control structure diagram for H$_\infty$ controller design

It is seen from Fig. 5 that *K* has a multi-input multi-output (MIMO) structure. The reference of the current controller is marked as $r = [i_{rd}^*, i_{rq}^*]$. The value of *r* is obtained from the outputs of the power controller, to satisfy different control objectives as studied in [8], [33]-[29]. The input vector of the controller *K* is $\boldsymbol{r} - \boldsymbol{y} = [i_{rd}^* - i_{rd}, i_{rq}^* - i_{rq}]$, marked as $\boldsymbol{v}$. The output vector of *K* is $[V_{rd}, V_{rq}]$, marked as $\boldsymbol{u}$. $\boldsymbol{r}$ is also regarded as an uncertain external disturbance, satisfying $\|\boldsymbol{r}\|_\infty \leq 1$. Together with $\boldsymbol{d}$, the external disturbance vector can be marked as $\boldsymbol{w} = [r, d]$. The output and input of the controller *K*, marked as $\boldsymbol{u}$ and $\boldsymbol{v}$, are shaped along with two weighting functions, marked as W_u and W_p.

The weighted controlled output is marked as $\boldsymbol{z} = [z_1, z_2]$. The block including the controlled system and weighting functions is called the shaped generalized plant model, marked as *P*. The block *P*, *K* and their interconnections constitute the closed-loop system, marked as *N*. The state space realization of *P* can be derived as,

$$\begin{bmatrix} y\Delta \\ z \\ v \end{bmatrix} = P(s)\begin{bmatrix} u\Delta \\ w \\ u \end{bmatrix} = \begin{bmatrix} P_{11}(s) & P_{12}(s) \\ P_{21}(s) & P_{22}(s) \end{bmatrix}\begin{bmatrix} u\Delta \\ w \\ u \end{bmatrix}$$
$$= \left[\begin{array}{cccccc|c} \Delta_1 & 0 & \dots & \dots & 0 & & 0 \\ 0 & \dots & \dots & \dots & 0 & & 0 \\ 0 & \dots & \dots & \Delta_{14} & 0 & & 0 \\ 0 & \dots & \dots & \dots & 0 & & W_u \\ 0 & \dots & \dots & W_p & -W_p G_s B_d & & -W_p G_s \\ \hline 0 & \dots & \dots & I & -G_s B_d & & -G_s \end{array}\right]\begin{bmatrix} u\Delta \\ w \\ u \end{bmatrix} \quad (4)$$

The block *N* is described as **z** = *N(s)***w**. *N(s)* is the closed-loop transfer function. *N(s)* can be obtained through the linear fractional transformation (LFT) between *P* and *K*. Based on (4) and define the system sensitivity function as $S = (I + G_s K)^{-1}$, *N(s)* is,

$$N(s) = \begin{bmatrix} N_{11}(s) & N_{12}(s) \\ N_{21}(s) & N_{22}(s) \end{bmatrix} = P_{11} + P_{12}K(I - P_{22}K)^{-1}P_{21}$$
$$= \begin{bmatrix} \Delta_1 & 0 & \dots & 0 \\ 0 & \dots & 0 & 0 \\ 0 & \dots & \Delta_{14} & 0 \\ 0 & \dots & W_u KS & -W_u KSG_s B_d \\ 0 & \dots & W_p S & W_p SG_s B_d \end{bmatrix} \quad (5)$$

The design of the H$_\infty$ optimal controller is to find a stabilizing function *K* to minimize the largest gain for any input direction from **w** to **z**, which is the peak of the singular value of the closed-loop transfer function *N(s)*, and can be described by an H$_\infty$ norm as,

$$\|N\|_\infty = \max_\omega \bar{\delta}(N(j\omega)) = \gamma_{\min} < \gamma \quad (6)$$

The optimal solution of (6) is marked as γ_{min}, which can be obtained by solving the standard two-Riccati formula [27]. The γ-iteration algorithm is adopted which defines a proper value $\gamma > \gamma_{min}$ to approach the optimal value γ_{min}, as an H$_\infty$ suboptimal problem. For a nominal system, γ can be set as 1.

B. Weighting functions design

Weighting functions can be regarded as filters to shape the uncertain perturbation of controller outputs and inputs. It is shown in Fig. 6, ***u*** and **v** are shaped along with two transfer functions W_u and W_p. It is seen from (5) that *KS* is shaped by W_u, where *KS* is the transfer function between *d* and the control signals. It is important to include *KS* as a mechanism for limiting the gain and bandwidth of the controller, and the size of *KS* is also important for robust stability [30]. As such, W_u regulates the controller bandwidth and system robust stability through shaping *KS*. W_p reflects ***v***, as a mechanism to influence the tracking performance of the external disturbance. W_u can be a constant gain. For a normalized system, a reasonable range of the W_u is satisfied as,

$$W_u \le 1 \quad (7)$$

Different values of W_u have little influence on the tracking performance of the controller as shown by the tracking error in Fig. 7. The bandwidth of the singular value curves from ***r*** to ***v*** with different W_u are all around 150Hz.

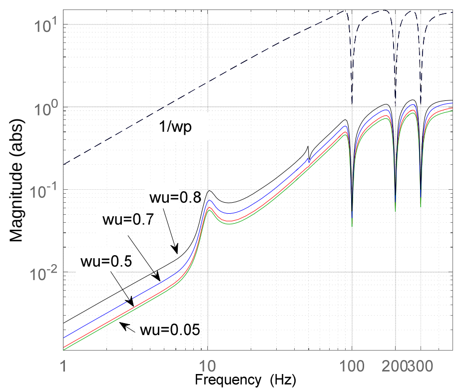

Fig. 7. Singular values from ***r*** to ***v*** with different W_u

The system stability is greatly influenced by W_u, as shown in Table I. With different values of W_u, the γ value varies. It is seen the γ value exceeds 1 when W_u is above 0.7, meaning the H$_\infty$ control requirement in (6) is no longer satisfied.

TABLE I
The ϒ value under different W_u

W_u	0.05	0.50	0.70	0.80
γ	0.07	0.45	1.44	2.53

As the reflection of the controller tracking performance, W_p must be designed to guarantee the tracking performance to the fundamental. A low pass filter is designed as the first part of W_p to shape the fundamental frequency characteristic,

$$W_{p1} = \frac{s/M + \omega_1}{s + \omega_1 A} \quad (8)$$

where the low-frequency gain of the tracking error, shaped as $1/|w_p(jw)|$, is *A*. The high-frequency gain of $1/|w_p(jw)|$ is *M*. The asymptote of the amplitude-frequency curve crosses 1 at ω_1. So the parameter tuning should satisfy $A \approx 0$ and $M \ge 1$ to limit the controller bandwidth. In order to guarantee the harmonic suppression performance, a band-pass filter with the resonance frequencies at the 2*nd*, 4*th* and 6*th* orders are introduced as the second part of W_p,

$$W_{p2} = \sum_{i=2,4,6} \frac{k_i \omega_i s}{s^2 + 2\xi_i \omega_i s + \omega_i^2} \quad (9)$$

where ω_i is the resonance frequency, ζ_i is the damping ratio, and k_i is the gain ratio. Based on (8) and (9), W_p is

$$W_p = W_{p1} + W_{p2} \tag{10}$$

The system closed-loop characteristic is obvious different with the parameter change of W_p. As Fig. 8 shows, with different ζ_i, the bandwidth of the closed-loop system varies from 200 Hz to 600 Hz.

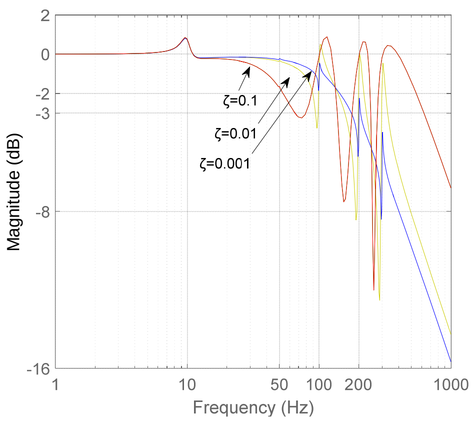

Fig. 8. Bode plots of the closed-loop response with different W_p

C. The RS and RP validation

The nominal system stability and control performance of H$_\infty$ controller is guaranteed by (6). For an uncertain model, the RS and RP should be further validated to guarantee system stability and satisfy control requirements with all the possible models, which can be validated by the structured singular value μ [30]. The system $N\Delta$-structure in Fig. 6 can be rearranged as a $M\Delta$-structure in Fig. 9, in which $M=N_{11}$.

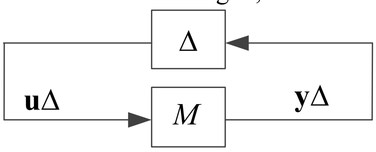

Fig. 9. $M\Delta$-structure diagram for μ analysis

The real non-negative function $\mu_\Delta(M)$, called the structured singular value, is obtained by the DK iteration [30]. The criteria of the RS and RP are given in (11). Δ_p is a full complex matrix.

$$\begin{cases} RS \Leftrightarrow \mu_\Delta(N_{11}) < 1, \forall \omega \\ RP \Leftrightarrow \mu_{\hat{\Delta}}(N) < 1, \forall \omega, \hat{\Delta} = \begin{bmatrix} \Delta & 0 \\ 0 & \Delta_p \end{bmatrix} \end{cases} \tag{11}$$

The parameters of the weighting functions are iteratively tuned to satisfy both the H$_\infty$ suboptimal bound in (6), and the RS and the RP properties determined by the structured singular value μ in (11). The parameters of the H$_\infty$ controller designed in this paper are listed in Table II.

TABLE II
Parameters of the weighting functions

A	M	ω_1	2nd	4th	6th	W_u
10^{-3}	15	800π	$\zeta_2 0.01$ $k_2 0.01$	$\zeta_4 0.01$ $k_4 0.01$	$\zeta_6 0.01$ $k_6 0.01$	0.5

Using the Matlab-Robust control toolbox with the μ-toolbox, the γ is calculated as 0.45, satisfying (6). The detailed closed-loop Bode plots of the designed H$_\infty$ controller with the possible uncertain models are given in Fig. 10. It is shown the bandwidth is more than 400 Hz for all the models, satisfying the control requirement. The tracking performance from i_{rd}^*, i_{rq}^* to i_{rd}, i_{rq}, as well as the damping performance from i_{rd}^*, i_{rq}^* to i_{rq}, i_{rd} at the resonant frequencies, are also guaranteed. The μ-curves of the RS and RP are shown in Fig. 11 and Fig. 12. All values in the μ-curves are smaller than 1, proving that the robustness of the designed H$_\infty$ controller is guaranteed for all the uncertain models.

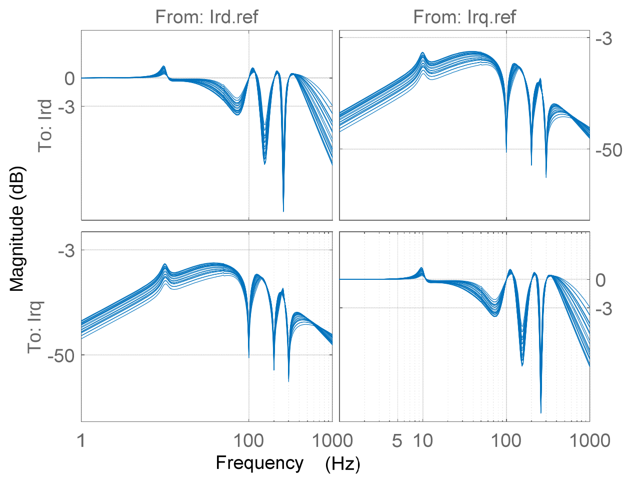

Fig. 10. Closed-loop Bode plots of the uncertain system by H$_\infty$ control

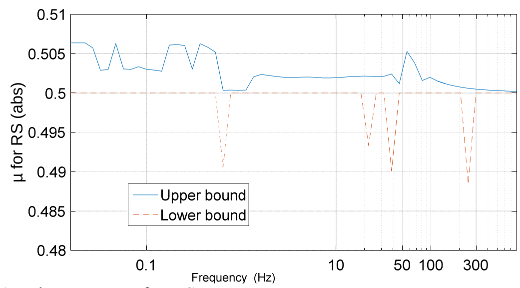

Fig. 11. The μ-curves for RS

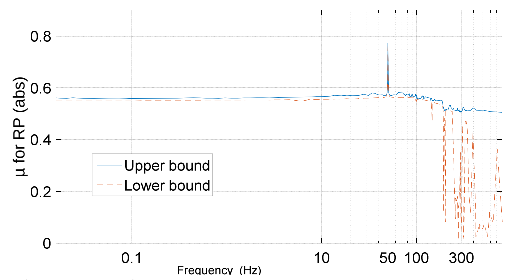

Fig. 12. The μ-curves for RP

IV. CASE STUDY

Case studies were performed using Matlab/Simulink Sim-Power Systems with a 1.5 MW DFIG WT model to verify the control performance of the H$_\infty$ rotor current controller. The control objective is to suppress rotor current distortions. The

PIR controller was also simulated to compare the performance. The wind speed was set as a constant of 15 m/s, and the reactive power reference was set as 0. The transfer function of the PIR controller is,

$$G_{PIR} = K_P + \frac{K_I}{s} + \sum_{i=2,4,6} \frac{K_{Ri} s}{s^2 + \omega_{ci} s + \omega_i^2} \qquad (12)$$

The parameters of the PIR current controller are tuned based on the frequency domain design method [15]. The parameters of the PIR controller are listed in Table III.

TABLE III
Parameters of the PIR controller

k_P	k_I	ω_{ci}	K_{R2}	K_{R4}	K_{R6}
6	0.8	10	300	300	300

A. Performance under grid background harmonics

From 3s to 3.3s, the grid background harmonics including 10% of the 5*th* harmonic and 10% of the 7*th* harmonic are added to the idea grid voltage. Fig. 13 shows the comparison of the rotor current with the H$_\infty$ control and the PIR control. Fig. 14 shows the results of the WT output power.

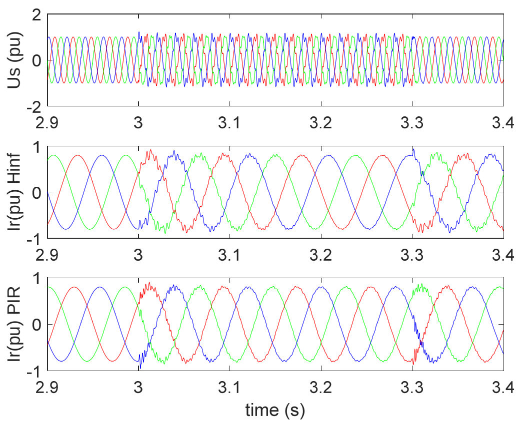

Fig. 13. Rotor current under grid background harmonics

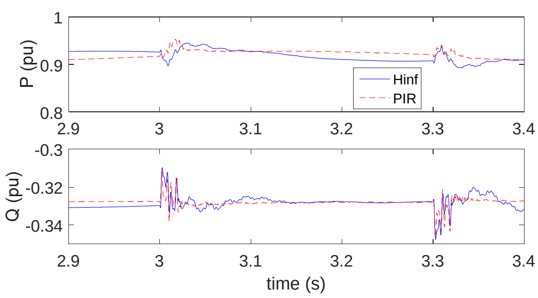

Fig. 14. Output power under grid background harmonics

It is seen from Fig.13 both the H$_\infty$ and PIR controllers can mitigate the 5*th* and 7*th* harmonics effectively. Table IV lists the FFT analysis results of i_{rd} from 3.1s to 3.2s. The results show the harmonic mitigation performance of the H$_\infty$ controller is better than the PIR controller. It is seen from Fig.14, the power oscillation at steady state by the H$_\infty$ and PIR current control has been decreased, while the dynamic performance of the output power by the H$_\infty$ controller is worse than the PIR controller.

TABLE IV
FFT analysis results of i_{rd} under grid harmonics

Type	200 HZ (%)	300 HZ(%)	*THD*(%)
H ∞	0.13	0.95	0.99
PIR	0.7	1.07	1.29

B. Performance under unbalanced grid voltage

A single phase to ground fault (phase A) with 30% dip depth was applied from 3s to 4s. Fig. 15 shows the comparison of the rotor current with the H$_\infty$ and PIR control. Table V lists the FFT analysis results of i_{rd} from 3.5s to 3.6s with the H$_\infty$ and PIR controllers, showing the H$_\infty$ controller with better harmonics suppression performance. Fig. 16 shows the results of the output power of wind turbine. It is seen the oscillation of the output power with the H$_\infty$ controller is more severe than the PIR controller. It is because the H$_\infty$ control focuses on the overall performance of the uncertain system with parameter perturbation. For the nominal model, the dynamic performance of the PIR control is better than the H∞ control.

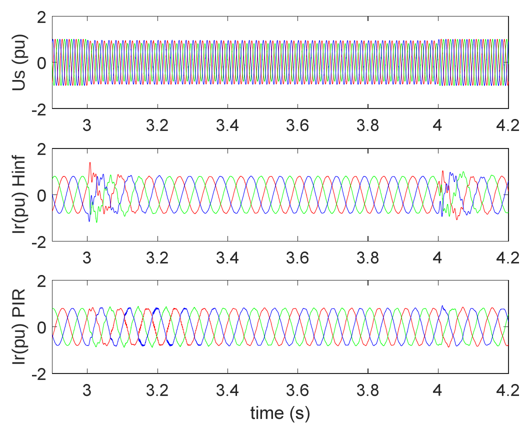

Fig. 15. Rotor current under asymmetric grid fault

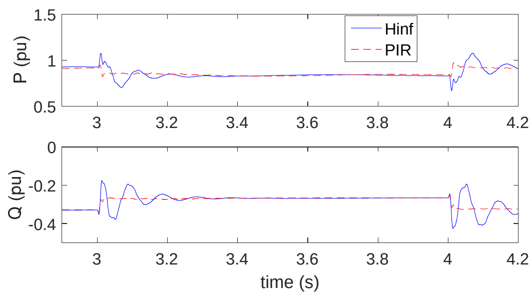

Fig. 16. Output power under asymmetric grid fault

TABLE V
FFT analysis results of i_{rd} under unbalanced grid voltage

Type	100 HZ (%)	*THD*(%)
H ∞	1.2	1.2
PIR	1.8	1.8

C. Performance with generator parameter perturbation

A single phase to ground fault (phase A) with 30% dip depth, and grid background harmonics with 10% of the 5*th* and 10% of the $7th$ order were applied from 3s to 4s. Fig. 17 shows the comparison of the rotor current with the H$_\infty$ and PIR control with the parameters of L_m, L_{ls}, L_{lr} and R_r all reduced to 70% of the nominal value. Fig. 18 shows the results of the WT output power. The FFT analysis results of i_{rd} with generator parameter perturbation from 3.5s to 3.7s are listed in Table VI. It can be seen from Fig. 17 that the performance of the H$_\infty$ controller is not much influenced by the parameter perturbation. The THD is 1.67% with the H$_\infty$ control, indicating the good tracking performance and robust stability with parameter perturbation. While for the PIR controller, the current control performance is obviously influenced by the parameter perturbation, with the THD being up to 10.79%.

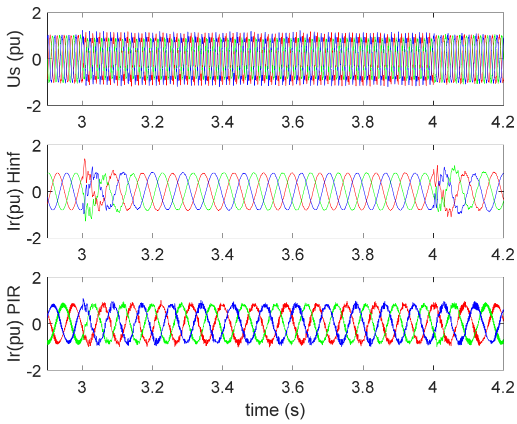

Fig. 17. Rotor current with parameter perturbation

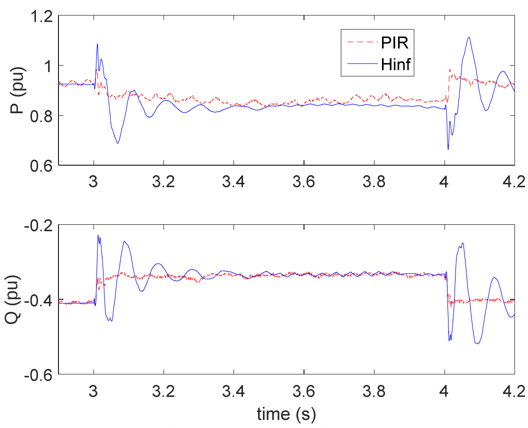

Fig. 18. Output power with parameter perturbation

TABLE VI

FFT analysis of i_{rd} under parameter perturbation and grid distortions

Type	1st (%)	2nd (%)	4th (%)	6th (%)	*THD*(%)
$H\infty$	0.36	1.2	0.63	0.65	1.67
PIR	0.18	2.50	1.98	1.68	10.79

Fig. 19 and Fig. 20 show the rotor currents with the H$_\infty$ and PIR control with L_m, L_{ls}, L_{lr} and R_r reduced to 50% of the nominal value. Fig. 19 shows the performance of H$_\infty$ controller is similar with the nominal model and the parameter perturbed model. The THD is 1.74% from 3.5s to 3.7s, and the system is stable, while it is seen from Fig. 20 that the system becomes unstable with the PIR control subject to the DFIG parameter perturbation.

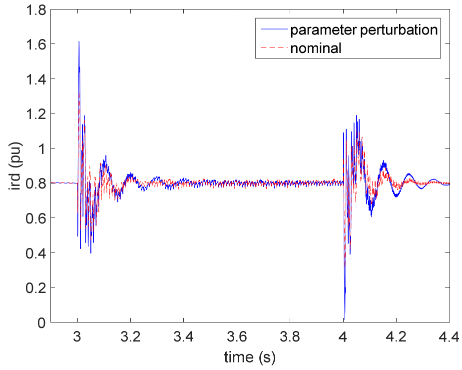

Fig. 19. i_{rd} under parameter perturbation by H$_\infty$ control

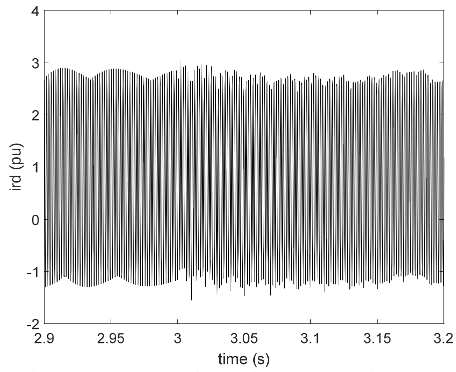

Fig. 20. i_{rd} under parameter perturbation by PIR control

The above simulation results show both the H$_\infty$ and PIR control have good harmonics suppression performance with the nominal model. The dynamic performance of the PIR controller with the nominal model is better than the H$_\infty$ controller. Under the parameter perturbed conditions, the stability and robust performance of the H$_\infty$ controller is better than the PIR controller.

V. Conclusion

In this paper, an H$_\infty$ robust controller was designed for the DFIG rotor current regulation in order to improve the robustness and harmonic suppression performance subject to grid voltage distortions and generator parameter perturbation. The H$_\infty$ controller is designed based on an uncertain MIMO DFIG model and the RS and RP of the H$_\infty$ controller is verified by the structured singular value μ. Case studies show that the designed H$_\infty$ controller can effectively suppress current harmonics with $2nd$, $4th$ and $6th$ orders under grid voltage distortions. The H$_\infty$ current controller can improve the robustness of the DFIG based wind turbine subject to grid voltage distortions, guarantee harmonics suppression performance as well as the stability with parameter perturbation.

The designed H$_\infty$ controller can also be applied to other WTs, such as PMSG based wind turbine with some modification of the controller parameters, and will be investigated in the future work. Experiments will also be conducted to validate the proposed control in the future work.

APPENDIX

TABLE VII
The parameters of 1.5 MW DFIG model

Rated power	1.5 MW
Stator voltage	0.69 kV
Electrical base frequency	50 Hz
Stator resistance	0.023 pu
Rotor resistance	0.016 pu
Stator leakage inductance	0.18 pu
Rotor leakage inductance	0.16 pu
Mutual inductance	2.9 pu
Nominal frequency	50 Hz

REFERENCE

[1] S. Liang, Q. Hu, and W. Lee, "A survey of harmonic emissions of a commercial operated wind farm," in *2010 IEEE Industrial and Commercial Power Systems Technical Conference - Conference Record*, 2010, pp. 1–8.

[2] M. Kiani, "Effects of Voltage Unbalance and System Harmonics on the Performance of Doubly Fed Induction Wind Generators," *IEEE Trans. Ind. Appl.*, vol. 46, no. 2, pp. 562–568, 2010.

[3] J. LÓpez, E. GubÍa, P. Sanchis, X. Roboam, and L. Marroyo, "Wind Turbines Based on Doubly Fed Induction Generator Under Asymmetrical Voltage Dips," *IEEE Trans. Energy Convers.*, vol. 23, no. 1, pp. 321–330, Mar. 2008.

[4] M. Tsili and S. Papathanassiou, "A review of grid code technical requirements for wind farms," *IET Renew. Power Gener.*, vol. 3, no. 3, p. 308, 2009.

[5] I. Erlich and U. Bachmann, "Grid code requirements concerning connection and operation of wind turbines in Germany," in *IEEE Power Engineering Society General Meeting, 2005*, 2005, pp. 2230–2234.

[6] S. Muller, M. Deicke, and R. W. De Doncker, "Doubly fed induction generator systems for wind turbines," *IEEE Ind. Appl. Mag.*, vol. 8, no. 3, pp. 26–33, 2002.

[7] H. Xu, J. Hu, and Y. He, "Operation of Wind-Turbine-Driven DFIG Systems Under Distorted Grid Voltage Conditions: Analysis and Experimental Validations," *IEEE Trans. Power Electron.*, vol. 27, no. 5, pp. 2354–2366, May 2012.

[8] L. Xu and Y. Wang, "Dynamic Modeling and Control of DFIG-Based Wind Turbines Under Unbalanced Network Conditions," *IEEE Trans. Power Syst.*, vol. 22, no. 1, pp. 314–323, Feb. 2007.

[9] E. Nasr-Azadani, C. A. Canizares, D. E. Olivares, and K. Bhattacharya, "Stability Analysis of Unbalanced Distribution Systems With Synchronous Machine and DFIG Based Distributed Generators," *IEEE Trans. Smart Grid*, vol. 5, no. 5, pp. 2326–2338, Sep. 2014.

[10] Jing Zhao, Wei Zhang, Yikang He, and Jiabing Hu, "Modeling and control of a wind-turbine-driven DFIG incorporating core saturation during grid voltage dips," *Electrical Machines and Systems, 2008. ICEMS 2008. International Conference on*. pp. 2438–2442, 2008.

[11] H. M. Jabr and N. C. Kar, "Effects of main and leakage flux saturation on the transient performances of doubly-fed wind driven induction generator," *Electr. Power Syst. Res.*, vol. 77, no. 8, pp. 1019–1027, Jun. 2007.

[12] R. Chattopadhyay, A. De, and S. Bhattacharya, "Comparison of PR controller and damped PR controller for grid current control of LCL filter based grid-tied inverter under frequency variation and grid distortion," in *2014 IEEE Energy Conversion Congress and Exposition (ECCE)*, 2014, pp. 3634–3641.

[13] Z. Li, Y. Li, P. Wang, H. Zhu, C. Liu, and F. Gao, "Single-Loop Digital Control of High-Power 400-Hz Ground Power Unit for Airplanes," *IEEE Trans. Ind. Electron.*, vol. 57, no. 2, pp. 532–543, Feb. 2010.

[14] W. H. Huang, X. X. Huo, S. J. Hu, and H. H. Xu, "Phase lead correction for VSI single-loop control," in *2013 IEEE International Conference on Applied Superconductivity and Electromagnetic Devices*, 2013, pp. 60–64.

[15] H. Nian and Y. Song, "Optimised parameter design of proportional integral and resonant current regulator for doubly fed induction generator during grid voltage distortion," *IET Renew. Power Gener.*, vol. 8, no. 3, pp. 299–313, Apr. 2014.

[16] H. Xu, J. Hu, H. Nian, and Y. He, "Dynamic modeling and improved control of DFIG under unbalanced and distorted grid voltage conditions," in *IEEE International Symposium on Industrial Electronics*, 2012, pp. 1579–1584.

[17] A. Susperregui, L. Xu, M. I. Martinez, and G. Tapia, "Sliding-mode control of a wind turbine-driven double-fed induction generator under non-ideal grid voltages," *IET Renew. Power Gener.*, vol. 7, no. 4, pp. 370–379, Jul. 2013.

[18] J. P. da Costa, H. Pinheiro, T. Degner, and G. Arnold, "Robust Controller for DFIGs of Grid-Connected Wind Turbines," *IEEE Trans. Ind. Electron.*, vol. 58, no. 9, pp. 4023–4038, Sep. 2011.

[19] Y. Song and H. Nian, "Sinusoidal Output Current Implementation of DFIG Using Repetitive Control Under a Generalized Harmonic Power Grid With Frequency Deviation," *IEEE Trans. Power Electron.*, vol. 30, no. 12, pp. 6751–6762, Dec. 2015.

[20] S. S. Choi, S. Wang, D. M. Vilathgamuwa, X. Zhang, and F. Wei, "Mitigation of distorted and unbalanced stator voltage of stand-alone doubly fed induction generators using repetitive control technique," *IET Electr. Power Appl.*, vol. 7, no. 8, pp. 654–663, Sep. 2013.

[21] H. Nian, P. Cheng, and Z. Q. Zhu, "Coordinated Direct Power Control of DFIG System Without Phase-Locked Loop Under Unbalanced Grid Voltage Conditions," *IEEE Trans. Power Electron.*, vol. 31, no. 4, pp. 2905–2918, Apr. 2016.

[22] J. Hu, J. Zhu, and D. G. Dorrell, "Predictive Direct Power Control of Doubly Fed Induction Generators Under Unbalanced Grid Voltage Conditions for Power Quality Improvement," *IEEE Trans. Sustain. Energy*, vol. 6, no. 3, pp. 943–950, Jul. 2015.

[23] M. P. S. Gryning, Q. Wu, M. Blanke, H. H. Niemann, and K. P. H. Andersen, "Wind Turbine Inverter Robust Loop-Shaping Control Subject to Grid Interaction Effects," *IEEE Trans. Sustain. Energy*, vol. 7, no. 1, pp. 41–50, Jan. 2016.

[24] Y. W. Li, D. M. Vilathgamuwa, F. Blaabjerg, and P. C. Loh, "A robust control scheme for medium-voltage-level DVR implementation," *IEEE Trans. Ind. Electron.*, vol. 54, no. 4, pp. 2249–2261, 2007.

[25] G. Willmann, D. F. Coutinho, L. F. A. Pereira, and F. B. Libano, "Multiple-Loop H-Infinity Control Design for Uninterruptible Power Supplies," *IEEE Trans. Ind. Electron.*, vol. 54, no. 3, pp. 1591–1602, Jun. 2007.

[26] M. Djukanovic, M. Khammash, and V. Vittal, "Application of the structured singular value theory for robust stability and control analysis in multimachine power systems. I. Framework development," *IEEE Trans. Power Syst.*, vol. 13, no. 4, pp. 1311–1316, 1998.

[27] J. C. Doyle, K. Glover, P. P. Khargonekar, and B. A. Francis, "State-space solutions to standard H/sub 2/ and H/sub infinity / control problems," *IEEE Trans. Automat. Contr.*, vol. 34, no. 8, pp. 831–847, 1989.

[28] V. Ignatova, P. Granjon, and S. Bacha, "Space vector method for voltage dips and swells analysis," *IEEE Trans. Power Deliv.*, vol. 24, no. 4, pp. 2054–2061, 2009.

[29] M. A. Asha Rani, C. Nagamani, G. Saravana Ilango, and A. Karthikeyan, "An Effective Reference Generation Scheme for DFIG With Unbalanced Grid Voltage," *IEEE Trans. Sustain. Energy*, vol. 5, no. 3, pp. 1010–1018, Jul. 2014.

[30] S. Skogestad and I. Postlethwaite, *Multivariable feedback control: analysis and design*, Vol. II. New York: WILEY, 2005.

[31] I. P. and E. Society, *IEEE Recommended Practice and Requirements for Harmonic Control in Electric Power Systems*, vol. 2014. 2014.